Eur. Phys. J. D (2011)
DOI: 10.1140/epjd/e2011-20503-7

THE EUROPEAN PHYSICAL JOURNAL D

Regular Article

Ordering of $SiO_xH_yC_z$ islands deposited by atmospheric pressure microwave plasma torch on Si(100) substrates patterned by nanoindentation

X. Landreau[1,a], B. Lanfant[1], T. Merle[2], E. Laborde[2], C. Dublanche-Tixier[1], and P. Tristant[1]

[1] SPCTS, ENSIL, 16 Rue Atlantis, Ester Technopole, 87068 Limoges, France
[2] SPCTS, CEC, 12 Rue Atlantis, Ester Technopole, 87068 Limoges, France

Received 29 August 2011 / Received in final form 10 October 2011
Published online 25 November 2011 – © EDP Sciences, Società Italiana di Fisica, Springer-Verlag 2011

Abstract. $SiO_xH_yC_z$ nanometric layers are deposited from hexamethyldisiloxane by atmospheric pressure microwave plasma torch on Si(100) substrates submitted to temperatures varying on the range [0 °C; 120 °C]. Atomic force microscopy (AFM) characterizations of samples grown at intermediate substrate temperatures (∼30 °C) demonstrate a layer-by-layer growth (Frank van der Merwe growth) leading to smooth flat and compact films while films deposited at lower and higher substrates temperatures show an island-like growth (Volmer-Weber growth) generating a high surface roughness. Concomitantly, a detailed infrared spectroscopy analysis of the growing films evidences structural modifications due to changes in the bond types, Si-O-Si conformation and stoichiometry correlated with scanning electron microscopy and AFM characterizations. Then, deposition conditions and specific microstructure are selected with the aim of generating 3-dimensional $SiO_xH_yC_z$ nanostructure arrays on nanoindented Si (100) templates. The first results are discussed.

1 Introduction

During the last decade, the development of arrayed silica nano-sensors has been the subject of intensive research for many applications in the scientific fields of medicine [1], particularly genomics [2], bio-diagnosis [3] and in the fields of material science [4,5]. At the present time, numerous methods have been developed for the formation of arrayed nanometer thick silicon dioxide dots including nanobiolithography techniques such as nanografting [6], dip-pen nanolithography [7], nanofountain pen nanolithography [8], or scanning near-field nanolithography [9]. However, all these methods are extremely time-consuming as they only allow the deposition of one dot at a time. Recently, numerous processes have demonstrated their ability to grow silicon oxide nanostructures in a highly speed and reproducible way [10–12] but the tailoring of their ordering remains a challenge. In this paper we aim to introduce an alternative and promising technique, based on atmospheric pressure plasma enhanced chemical vapor deposition (AP-PECVD) process, for the simultaneous deposition of silicon oxide nano-islands in a reduced time (a few seconds) and their ordering in a squared array. Firstly, substrate temperature conditions leading to nano-island growth are investigated by AFM and results are used for the deposition on prepatterned Si (100) substrates, with a self-organization objective. Then, the chemical structure (bond types, Si-O-Si conformation and stoichiometry) of the $SiO_xH_yC_z$ deposits is analyzed in detail by Fourier Transformed Infra-Red (FTIR) spectroscopy. Information about the specific surface and internal porosity are correlated with AFM observations.

[a] e-mail: xavier.landreau@ensil.unilim.fr

2 Experimental

2.1 Deposition process: the axial injection torch

The experimental apparatus consists of a 2.45 GHz microwave plasma TIA (Torche à Injection Axiale). The microwaves generated by a magnetron (600 W) are delivered to the flowing gas in a metallic coaxial tube, through a rectangular waveguide. The absorption of microwave energy in the flowing gas results in formation and sustention of plasma at the exit nozzle. The torch is placed in a large cylindrical deposition chamber. The substrate is fixed perpendicular to the plasma flow at a constant value of 30 mm. The reactor is equipped with an exhaust at the top to ensure the removal of products. A scheme of the PECVD system is shown in Figure 1. 30 sccm of Ar carrier gas is saturated with hexamethyldisiloxane (HMDSO), by passing through a bubbler under 3.5×10^5 Pa, it is mixed with the Ar plasma gas (16 standard liter per

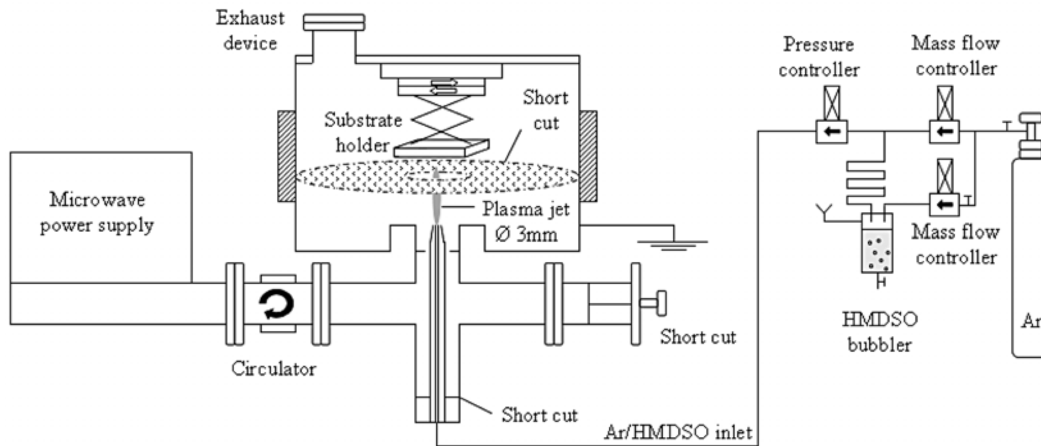

Fig. 1. Experimental set-up: geometry of the TIA.

minute – slpm) before entering in the torch through the inner conductor and creates a plasma of length 30 mm at the exit nozzle (diameter 3 mm) by coupling with the microwaves. The substrate temperature is controlled by a cooling system in the range [0 °C; 120 °C]. The deposition process is carried out during only 5 s in order to obtain nanometric thicknesses (∼30 nm) [13]. All experiments are made at normal laboratory environmental conditions (20 °C, 40% humidity).

2.2 Materials and methods

The nanometric silicon oxide films are deposited keeping the substrate stationary in front of the plasma. Before deposition, the substrates, which are a quarter of a 100 mm diameter (100) monocrystalline silicon wafer, are cleaned in a fluorydric acid solution in order to remove the native SiO_x nanometric layer. Then they are washed with ethanol in an ultrasonic bath during 15 min. This protocol allows to obtain a good surface roughness reproducibility both within and between the different substrates. During deposition, the substrate temperature is regulated by a homemade Peltier cooler device (Z02T21MD, Selectronic, $40 \times 40 \times 3.8$ mm) [13] with a precision of 4 °C during the first minute of deposition and of 2 °C after. The surface temperatures are measured with a monochromatic pyrometer (type IRCON mini RT 430-18 F-4) operating in the range of wavelengths [4 μm–12 μm] and corresponding to the scale of temperature [−28 °C; 982 °C]. The viewing angle from the vertical is 60°. The process gases and the precursor display an adequate purity (argon: Nital, 5.0 purity, HMDSO: liquid at standard conditions, Alfa Aesar, 98%). Surface morphology is investigated by atomic force microscopy (AFM, Scientec Multimode) in tapping mode and scanning electron microscopy (SEM, Philips XL 30). Fourier transformed infrared spectroscopy in transmission mode (T-FTIR, Nicolet 6700, resolution of 2 cm^{-1}) analyses are performed at the centre area of the deposits. Spectra deconvolutions into Gaussian profiles are realised using the OMNIC software and Origin Pro 7.5. Intensities of each band are normalized from the TO_1 mode intensity in order to avoid the contribution of the film thickness and to estimate the proportion of different chemical species contained within the film. Moreover, the reported data correspond to an average value of 6 repetition samples. Then, squared arrays of indents on Si (100) substrates are patterned at room temperature using a nanoindenter XP^{TM} (MTS Nano Instruments) with a Berkovich diamond tip. Residual impressions are ∼200 nm deep and of ∼2 μm diameter with center-to-center pitches of 2 μm.

3 Results

3.1 AFM analyses

Figure 2 presents 3D AFM images of nanometer thick films deposited under different substrate temperatures: 0 °C, 30 °C, 60 °C, 90 °C and 120 °C. At 30 °C (Fig. 2b), the SiO_x layer covers the Si surface uniformly with almost no rugosity over several 5 μm × 5 μm samples. However, layers deposited at other temperatures (Figs. 2a, 2c–2e) reveal the growth of 3D SiO_x self-assembled nano-islands. This interesting observation reasonably agrees with the predicted effect of the surface diffusion as a control mechanism of the resulting morphology: the transition from an ambient substrate temperature to lower and higher temperatures causes a change in the growth mechanisms. As reported elsewhere [13,14], this change basically results from the Frank van der Merwe (FM) growth (layer-by-layer) or the Volmer-Weber (VW) growth (island growth) due to a modification of the ratio value ϕ/k_BT (where ϕ denotes the diffusion barrier potential, T the surface temperature and k_B the Boltzmann constant) [15,16]. At very low substrate temperature T, the adparticles have practically no mobility since they cannot overcome the diffusion barrier potential: they stick to the growing film at the same place where they hit it ("hit-and-stick" or "ballistic" deposition [17]) and a dot-like structure separated by voids develops. At high temperatures, the mobility is enhanced but the probability that diffusing adparticles encounter impinging particles increases. As a consequence,

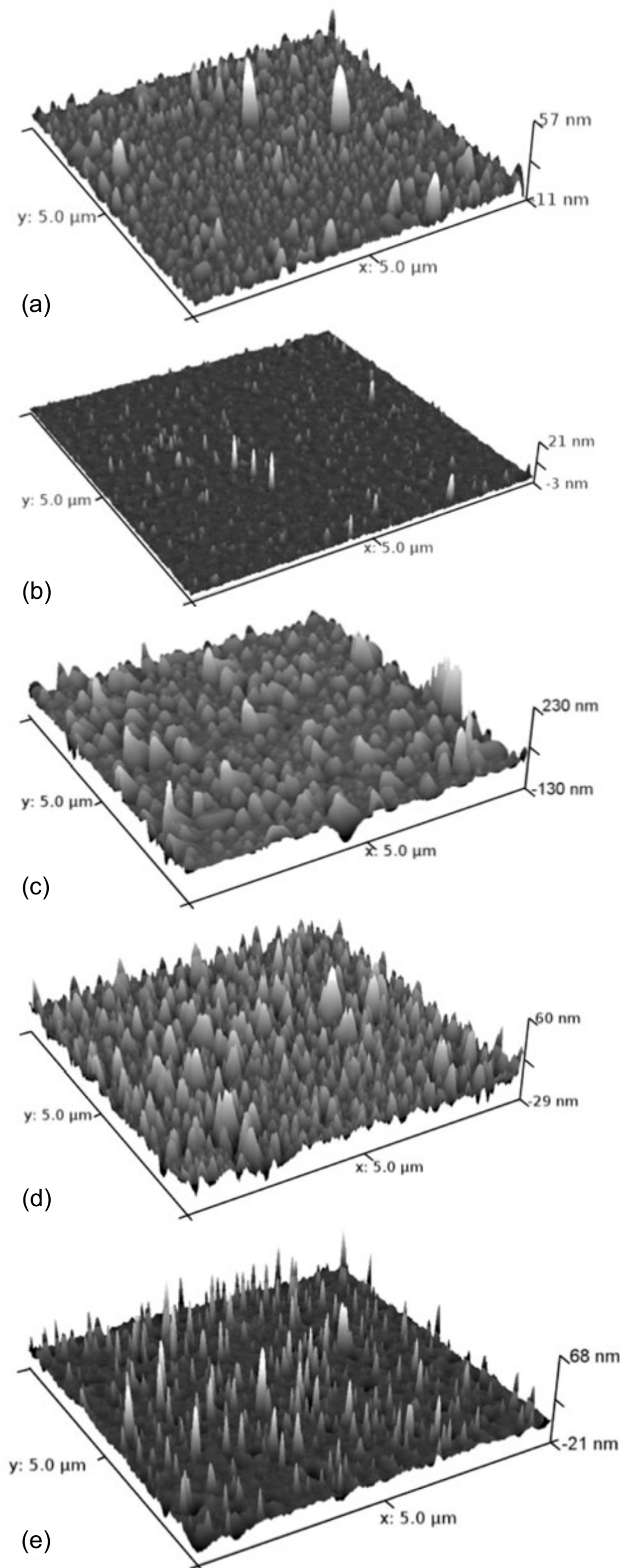

Fig. 2. Atomic force microscopy images of SiO_x layers deposited during 5 s at (a) 0 °C, (b) 30 °C, (c) 60 °C, (d) 90 °C and (e) 120 °C. No matter between nano-islands is supposed because the measured inter-dots rugosity is comparable to the substrate rugosity: ∼5 Å. Average island heights estimated by AFM over 6 repetition samples are (a) ∼15 nm, (c) ∼35 nm, (d) ∼25 nm, (e) ∼20 nm (dispersion ⩽10%).

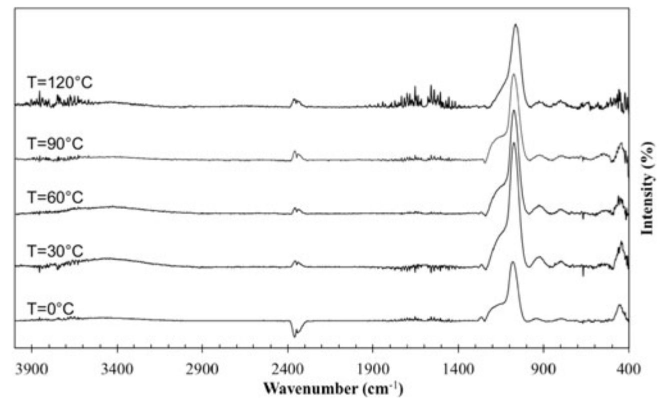

Fig. 3. FTIR specular reflexion spectra of nanometric $SiO_xH_yC_z$ films deposited at five different substrate temperatures.

intermolecular bonds can develop to grow stable clusters and the mean surface diffusion length λ_D decreases (λ_D is also limited by the desorption). As coverage increases, the cluster size rises and λ_D decreases again causing thermal roughening [15]. After a short time, stable nano-hillocks strongly attract molecules diffusing in the vicinity ("capture zone concept" [18]). Finally, as reported by Xiao et al. [15,16], λ_D has optimal values at intermediate substrate temperatures, which results in a smooth flat surface due to a layer-by-layer growth, as observed Figure 2b.

3.2 FTIR and XPS analyses: correlations with AFM observations

Figure 3 presents the evolution of FTIR spectra obtained in specular reflexion mode with rising temperature on the range [0 °C; 120 °C]. All spectra exhibit the characteristic features of amorphous silicon oxide films, namely $\delta_{\text{Si-O-Si}}$, $\gamma_{\text{Si-O-Si}}$, and $\nu_{as\ \text{Si-O-Si}}$ at 460, 805 and 1075 cm^{-1} respectively [19,20]. The band associated to the Si-$(CH_3)_x$ bonds (1270 cm^{-1}) appears at all temperatures except at 90 °C. However, the bands related to C-H vibrators in the vicinity of 2950 cm^{-1} are not detected. Bands associated to free (or geminated) OH and H_2O groups are difficult to interpret because of a high background above 3400 cm^{-1}. Nevertheless, the signal corresponding to Si-OH bonds (940 cm^{-1}) is very clear for each temperature and can be used for semi-quantitative estimations.

Deconvolution of the ASM band (asymmetric stretching mode, ∼1000–1300 cm^{-1}) into Gaussian profiles (Fig. 4) gives rise to additional bands compared to those obtained in the case of films recorded at normal incident radiations. Indeed, at oblique incidence radiation, the longitudinal modes occur (Berreman effect [21]) and the ASM absorption band of a crystalline silicon dioxide film is split into two modes (TO_1, LO_1) of frequencies close to 1075 and 1250 cm^{-1} [19,20,22]. Similarly in the case of amorphous silicon oxide films, in addition to these two components, four more modes can emerge in the ASM band with maxima at around 1050, 1150, 1200, and 1300 cm^{-1}

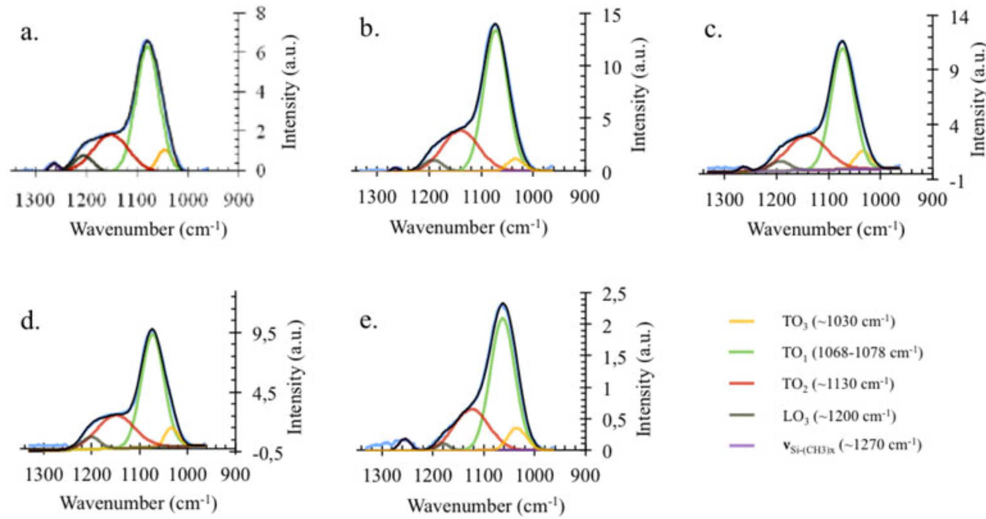

Fig. 4. (Color online) FTIR specular reflexion spectra of the $SiO_xH_yC_z$ films: deconvolution of the Si-O-Si ASM band profile into four modes of the SiOSi group. Qualitative analysis of the structure variations with rising temperature.

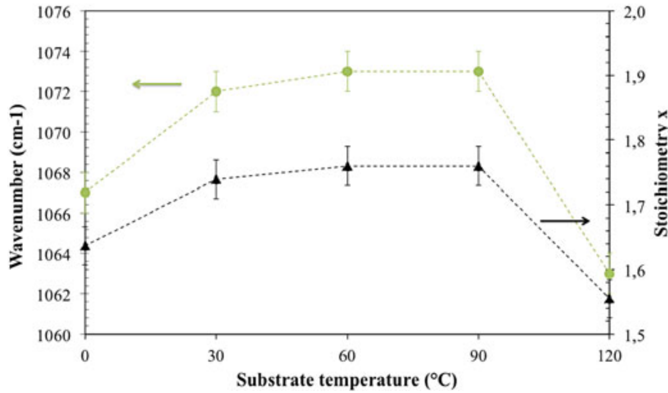

Fig. 5. (Color online) Evolution of the stoichiometry x in SiO_x films with rising temperature according to the TO_1 mode wavenumber variations [28].

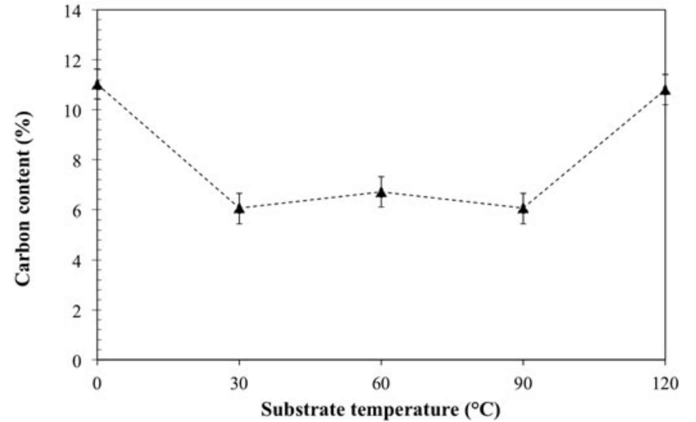

Fig. 6. Carbon content variations in the deposited films measured by XPS with rising substrate temperature: correlation with stoichiometry constant x variations of Figure 5.

(corresponding to TO_3, TO_2, LO_3, LO_2 respectively). According to [19,23], the TO_1 mode at $\sim$1075 cm^{-1} reflects a quartz-like structure with a constant bond angle of $\theta = 144°$ in a sixfold ring configuration while the TO_3 mode ($\sim$1050 cm^{-1}) corresponds to planar threefold rings or packed fourfold rings configurations associated with a bond angle close to $\theta = 120°$ (coesite-like structure). Then, a β-cristobalite-like structure revealed by a TO_2 mode at $\sim$1150 cm^{-1} is associated with the higher bond angle $\theta = 180°$ [24]. This last mode, sometimes called surface mode [14,25,26], is characteristic of the specific surface within the film because of the numerous obtuse bond angles contained on the extreme surface.

In Figure 4, the first band detected at $\sim$1195 cm^{-1} corresponds to the LO_3 mode. This band has a low intensity and no significant variations with rising temperature, which is coherent with observations of [27]. A second band, centred at $\sim$1030 cm^{-1}, corresponding to the TO_3 mode [19] demonstrates the presence of $\theta_{\text{Si-O-Si}}$ angles closed to 120° and reflects a relative disorder in the SiO_4 tetrahedra compared to a crystalline silica structure.

Figure 5 reports the evolution of the central position of the TO_1 mode (1068–1078 cm^{-1}). The spectral shift of this band is an indication of the stoichiometry of the SiO_x films [28]. The blue shift indicates a higher stoichiometry constant x. Maximum values are obtained in the temperature range [30 °C; 90 °C] and correspond to $x = 1.75$. This observed trend is clearly supported by X-ray photoelectron spectroscopy (XPS) measurements (Fig. 6), which demonstrate a minimum carbon content in the same temperature interval. Moreover, the low intensity variations of the band associated to Si-OH groups (940 cm^{-1}) (Fig. 7) attest that carbon is the main factor causing the stoichiometric transition at intermediate temperatures. These carbon content variations could be indirectly explained by a change in the growth mechanisms. In the case of a 3D-growth, the bonds between atoms or molecules constituting the film are stronger than the bonds created with

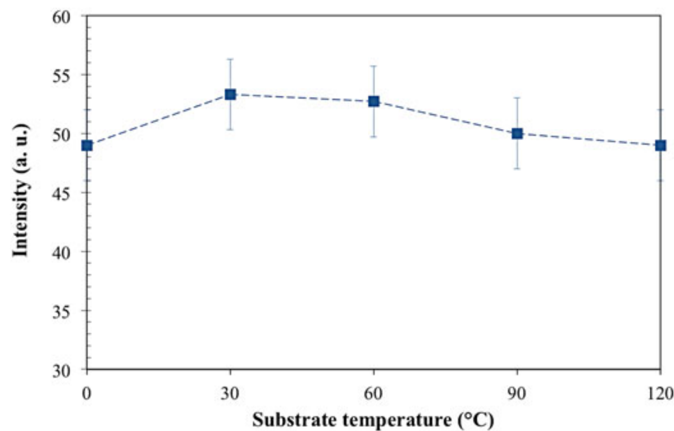

Fig. 7. (Color online) Estimation of the Si-OH content with rising temperature.

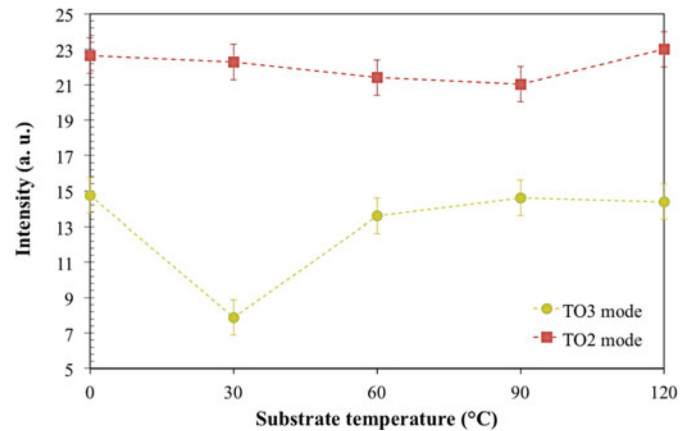

Fig. 8. (Color online) Evolution of the TO_3 and TO_2 mode intensity with rising substrate temperature: correlations with surface morphology (Fig. 2).

the substrate. Therefore a competitive effect between the desorption of radical carbon species and the attraction between the adsorbed species and the stable islands could occur. In our case, this competition would lead to incorporation of carbon in the islands and an increase in their concentration in the whole layer. However, this hypothesis remains to be validated.

As far as the TO_2 mode is concerned, very low intensity variations are noticeable (Fig. 8), which is not a priori coherent with surface topography variations recorded by AFM (Fig. 2): we expected to observe a decrease in the mode intensity for the 30 °C sample, but it is not the case. Thus it can be supposed that this mode is not significant in the case of nanometer dimension SiO_x films. Contrary to the TO_2 mode, the TO_3 mode exhibits noteworthy variations, which can be correlated to the surface morphology changes. Indeed, the presence of 3-dimensional nano-dots seems to cause prominent amplitude of the TO_3 mode. This would imply that the corresponding island-like structures are mainly composed of planar threefold rings or packed fourfold rings associated to a bond angle θ close to 120 °C [19,23]. This result is in accordance with observations reported by the authors of [29]. Indeed, they demonstrated that the contribution of TO_3 is very dependent on the thickness: particularly, it was established that the TO_3 mode has a higher activity in the case of thin films while the TO_1 mode often dominates in thick films [30,31]. This implies that the oscillators are distributed nonuniformly over the thickness: the ratio of planar threefold/sixfold ring is higher for the first oxide layers.

4 Spatial organization of $SiO_xH_yC_z$ nano-islands

In this part, the substrates are patterned prior to $SiO_xH_yC_z$ deposition by nanoindentation (Fig. 9a) with the aim that the nanoindents act as energetic trapping sites, enhancing diffusion of adatoms on their surface and ripening of $SiO_xH_yC_z$ islands at those locations. Moreover, since spatial island equilibration is triggered by surface diffusion, optimum ordering occurs when the pattern pitch is comparable to the surface diffusion length λ_D. According to results obtained in 3.1 and previously [13], λ_D of $SiO_xH_yC_z$ reaches an optimal value (roughly estimated to 1 μm) when the surface temperature is close to 30 °C. Thus, deposition is performed during 5 s at a substrate temperature of 30 °C, on a substrate patterned by a 2 μm – pitch indent squared array.

Figures 9b–9f show the surface morphology of indents observed by SEM after the initial stages of $SiO_xH_yC_z$ deposition and dot assembly. We observe that large hemispherical $SiO_xH_yC_z$ islands of mean diameter ≈150 nm nucleate inside the indents. Some matter also remains trapped in and between the indents: in particular, smaller dots gather at the edges and on the sidewall slope of the pits. These observations reasonably agree with theoretical predictions of reference [32], suggesting that inside the indents the island formation energy is smaller than on the flat surface, due to an enhanced strain relaxation: because of a higher coordination number, adatoms located at the bottom of an indent (or an edge in a simple case) find a more stable position than those located on a smooth and flat surface. Indeed, each atom reaching at least one edge of an indent can relax to the extent that it finds at least two nearest neighbours within the atoms belonging to the substrate or to an existing island [33]. That way, the potential energy barrier for adparticles extraction and diffusion outside such favorable adsorption site is strongly increased.

However, in addition to a pure geometrical effect of the indent, a second effect due to an island already present can greatly modify the diffusion within the indent. Such phenomena, known as Otswald ripening [34,35], is the process by which larger particles grow at the expense of smaller one. After the initial nucleation stage, the molecular clusters exceeding a critical size continue to grow and attract molecules moving on the surface. Then, the islands may progressively grow through large island–small island interactions: the most stable islands can develop a capture zone [18] where the wandering molecules are strongly

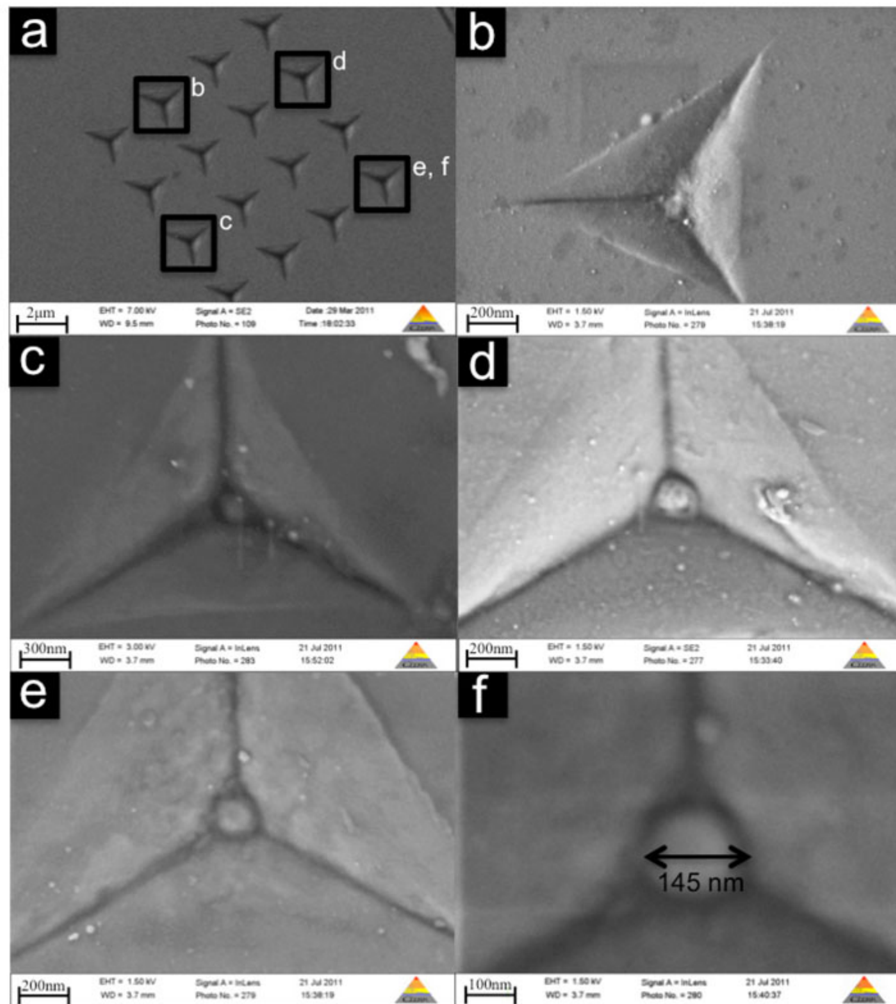

Fig. 9. (Color online) SEM images of the surface morphology of $SiO_xH_yC_z$ nano-islands localized at the center of nano-indents after 5 s of deposition with a substrate temperature of 30 °C.

attracted. In our case, the stable islands located at the center of the indents represent the most favourable energetic sites for new impinging molecules or for small adparticles already present.

SEM images of films deposited at substrate temperatures higher and lower than 30 °C confirm the results obtained by AFM characterization. An example is given in Figure 10a for a 5 s deposit realized at 90 °C: we observe that nano-dots uniformly cover the surface without preferential nucleation at the centre of the indent, which is consistent with the results of Figure 2d. As reported by Kamins et al. [36], the surface diffusion length during nucleation can be roughly estimated to be half the center-to-center island spacing. In Figure 10a, the average captured λ_D is about 0.25 μm, which is much lower than the pattern pitch; this sets the lower limit of pitch below which corner of indents can overlap.

Another interesting result concerns the $SiO_xH_yC_z$ films deposited at 30 °C substrate temperature for deposition time higher than 5 s: in Figures 10b–10d for deposition time of 10 s, 15 s and 20 s respectively, we observe that the matter, at latter stages, not only remains trapped but also moves out of the pits from the corners and assemble on terraces around them (Fig. 10b). This process, which has already been observed in the case of Ge material [37], seems to continue until a complete filling of the indent and a total covering of the substrate (Figs. 10c and 10d).

5 Conclusion

The deposition of continuous and discontinuous nanometric $SiO_xH_yC_z$ films from HMDSO is achieved by means of an atmospheric pressure microwave plasma torch (TIA) on Si (100) substrates. By varying the substrate temperature on the range [0 °C; 120 °C], we observe a change in the growth mechanism resulting from a Frank van der Merwe growth at intermediate substrate temperatures and a Volmer-Weber growth at other temperatures. The observed results are consistent with the predicted effects of surface diffusion as a control mechanism for the resulting

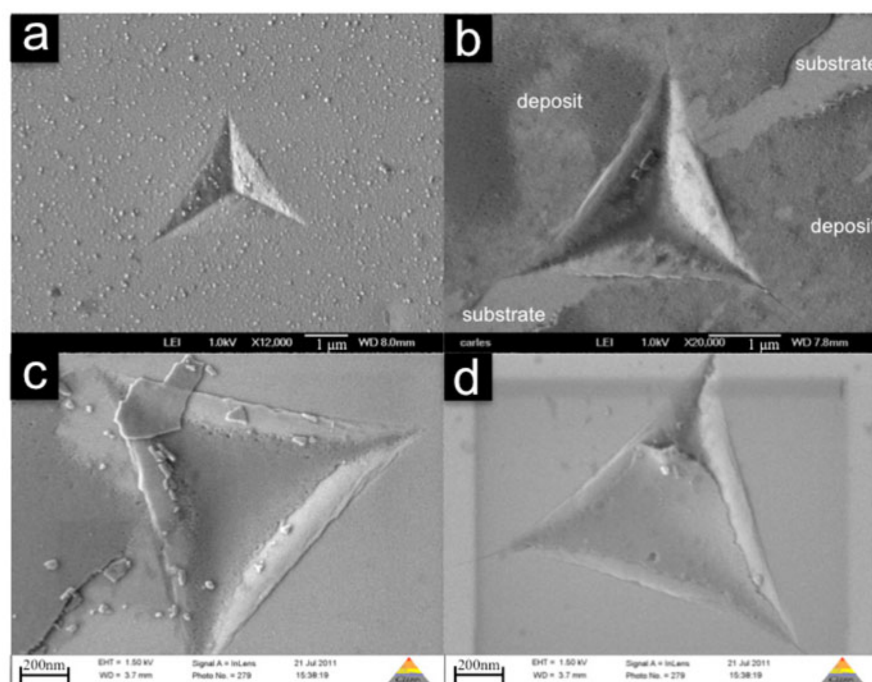

Fig. 10. (Color online) (a) Surface morphology of $SiO_xH_yC_z$ nano-islands after 5 s of deposition at $T_{\text{substrate}} = 90$ °C; $SiO_xH_yC_z$ deposit at $T_{\text{substrate}} = 30$ °C for a deposition time of (b) 10 s, (c) 15 s and (d) 20 s.

surface morphology. FTIR spectroscopy and XPS analyses demonstrate that intermediate substrate temperatures lead to films containing a lower carbon content ($x = 1.75$) while other temperatures generate a higher carbon contamination ($x < 1.6$), probably due to an indirect effect of substrate temperature on decomposition mechanisms in plasma phase or/in the transition sheath. Contrary to the carbon, the amount of –OH groups remains relatively stable with substrate temperature modifications. Concomitantly to the stoichiometric transition, numerous changes in the microstructure occur: discontinuous films (Volmer-Weber growth) deposited at low and high substrate temperature are mainly composed of planar threefold rings or packed fourfold rings associated to a Si-O-Si bond angle close to 120 °C, which is not the case at intermediate temperatures. Then, we report the ordering of $SiO_xH_yC_z$ islands grown on Si (100) substrates patterned by nanoindentation for a substrate temperature of 30 °C. Referring to the deviation of the spatial distribution of the $SiO_xH_yC_z$ islands from pure randomless, we conclude that indents act as preferred nucleation sites. In the absence of detailed data on the early stages of the nucleation, we can only speculate that the mobility of $SiO_xH_yC_z$ islands on the slope of the pits or at the pit edges is affected by the local minimum energy to such degree as to favor the bonding in the edges.

Further work should concentrate on a more precise FTIR analysis of the OH band (3000–3700 cm^{-1}) in order to distinguish and estimate the content of the different type of OH groups (free, geminated, H-bonded), which will provide useful information on the dots reactivity for later functionalization in nanosensing devices.

References

1. J.H. Lim, D.S. Ginger, K.B. Lee, J. Heo, J.M. Nam, C.A. Mirkin, Angew. Chem. Int. Ed. **42**, 2309 (2003)
2. Y.L. Wua, J.J. Lin, P.Y. Hsua, C.P. Hsu, Sens. Actuators B **155**, 709 (2011)
3. A. Bruckbauer, D.J. Zhou, L.M. Ying, Y.E. Korchev, C. Abell, D. Klenerman, J. Am. Chem. Soc. **125**, 9834 (2011)
4. B. Fousseret, M. Mougenot, F. Rossignol, J.F. Baumard, B. Soulestin, C. Boissière, F. Ribot, D. Jalabert, C. Carrion, C. Sanchez, M. Lejeune, Chem. Mater. **22**, 3875 (2010)
5. K. Teshima, Y. Inoue, H. Sugimura, O. Takai, Thin Solid Films **420-421**, 324 (2002)
6. K. Wadu-Mesthrige, S. Xu, N.A. Amro, G.Y. Liu, Langmuir **15**, 8580 (1999)
7. R.D. Piner, J. Zhu, F. Xu, S.H. Hong, C.A. Mirkin, Science **283**, 661 (1999)
8. H. Taha, R.S. Marks, L.A. Gheber, I. Rousso, J. Newman, C. Sukenik, A. Lewis, Appl. Phys. Lett. **83**, 1041 (2003)
9. S.Q. Sun, M. Montague, K. Critchley, M.S. Chen, W.J. Dressick, S.D. Evans, G.J. Leggett, Nano Lett. **6**, 29 (2006)
10. G. Arnoult, T. Belmonte, F. Kosior, M. Dossot, G. Henrion, J. Appl. Phys. **44**, 174022 (2011)
11. I. Levchenko, U. Cvelbar, K. Ostrikov, Appl. Phys. Lett. **95**, 021502 (2009)
12. K. Ostrikov, I. Levchenko, U. Cvelbar, M. Sunkara, M. Mozetic, Nanoscale **2**, 2012 (2010)
13. X. Landreau, C. Dublanche-Tixier, C. Jaoul, C. Le Niniven, N. Lory, P. Tristant, Surf. Coat. Technol. **205**, 335 (2011)
14. J. Schäfer, R. Foest, A. Quade, A. Ohl, J. Meichsner, K.D. Weltmann, Eur. Phys. J. D **54**, 211 (2009)
15. R.F. Xiao, N.B. Ming, Phys. Rev. E **49**, 4720 (1994)

16. R.F. Xiao, J.I.D. Alexander, F. Rosenberger, Phys. Rev. A **43**, 2977 (1991)
17. S. Mahieu, P. Ghekiere, D. Depla, R. De Gryse, Thin Solid Films **515**, 1229 (2006)
18. S. Pratontep, M. Brinkmann, Phys. Rev. B **69**, 165201 (2004)
19. I.P. Lisovskii, V.G. Litovchenko, V.G. Lozinskii, G.I. Steblovskii, Thin Solid Films **213**, 164 (1992)
20. M.K. Gunde, Physica B **292**, 286 (2000)
21. D.W. Berreman, Phys. Rev. **130**, 2193 (1963)
22. R.A.B. Devine, Appl. Phys. Lett. **68**, 3108 (1996)
23. S.S. Kilchitskaya, S.V. Litvinenko, V.A. Skryshevsky, V.I. Strikha, V.P. Tolstoy, Poverhnost (Surface) **4**, 99 (1987)
24. V.V. Tarasov, *Problems of Glass Physics* (Stroiizdat, Moscow, 1979)
25. J. Schäfer, R. Foest, A. Quade, A. Ohl, K.D. Weltmann, Plasma Process. Polym. **6**, S519 (2009)
26. J. Schäfer, S. Horn, R. Foest, R. Brandenburg, P. Vasina, K.D. Weltmann, Surf. Coat. Technol. **205**, S392 (2011)
27. A. Brunet-Bruneau, J. Rivory, B. Rafin, J.Y. Robic, P. Chaton, J. Appl. Phys. **82**, 1330 (1997)
28. P.G. Pai, S.S. Chao, Y. Takagi, G. Lucovsky, J. Vac. Sci. Technol. **4**, 690 (1986)
29. V.A. Skryshevsky, V.P. Tolstoy, *Infrared Spectroscopy of Semiconductor Structures* (Lybid, Kiev, 1991)
30. A. Slaoui, J.P. Ponpon, P. Siffert, Appl. Phys. **43**, 301 (1987)
31. E.M. Allegretto, J.A. Bardwell, J. Vac. Sci. Technol. **14**, 2437 (1996)
32. H. Hu, H.J. Gao, F. Liu, Phys. Rev. Lett. **101**, 216102 (2008)
33. Z. Zhang, M.G. Lagally, Science **276**, 377 (1997)
34. W. Oswald, Phys. Chem. **34**, 495 (1900)
35. B.K. Chakraverty, J. Phys. Chem. Solids **28**, 2401 (1967)
36. T.I. Kamins, E.C. Carrs, R.S. Williams, S.J. Rosner, J. Appl. Phys. **81**, 211 (1997)
37. Z. Zhong, O.G. Schmidt, G. Bauer, Appl. Phys. Lett. **87**, 133111 (2005)